Parametric Spring Reverberation Effect*

VESA VÄLIMÄKI, *AES Member*, **AND JULIAN PARKER**
(vesa.valimaki@tkk.fi) (julian.parker@tkk.fi)

Department of Signal Processing and Acoustics, Aalto University School of Science and Technology, Espoo, Finland

AND

JONATHAN S. ABEL, *AES Fellow*
(abel@ccrma.stanford.edu)

CCRMA, Department of Music, Stanford University, Stanford, CA 94305, USA

A parametric modeling technique for emulating spring reverberation units is developed. A spectral delay filter consisting of a cascade of identical all-pass filters implements the chirplike initial response. A feedback loop containing a randomly modulated delay line produces multiple echoes of the initial pulse, which are progressively blurred over time to produce the reverberant tail of the response. The calibration of model parameters from measurements and from analytic results is shown.

0 INTRODUCTION

Spring reverberation was an early form of artificial reverberation, first proposed by Hammond in the 1930s as a method for adding a more acoustic quality to the sound of his electromechanical organs [1]. Over the next several decades the compact nature and low cost of this technique led to its wide adoption both within studio environments and integrated into amplification systems for live performance. The sound produced by a spring reverberation unit has a distinctive quality, similar to, but unlike that produced by either a real acoustic space or other artificial reverberation techniques. This unique quality, and its historical importance to a number of musical genres, have led to demand for methods of reproducing the sound of spring reverberation in a modern digital-audio context.

A number of previous attempts at producing a digital model of spring reverberation have been made. The first of these attempts was based on digital-waveguide techniques in combination with the optimization of a high-order all-pass filter to fit measured data from a spring reverberation unit [2], [3]. Later work has concentrated on the discretization of a continuous model of spring vibration via finite difference techniques [4], [5]. There is a large body of related earlier work in the field of artificial reverberation. Parametric models for the simulation of room reverberation have been developed since the 1960s [6]–[9]. Gardner has written an excellent review of digital reverberation algorithms [10]. Recently other historical reverberation techniques have been simulated using digital techniques, such as plate reverberators [11], [12] and a tape delay unit [13].

In this paper we aim to approach the problem of modeling spring reverberation from a different perspective. We use techniques familiar from other forms of digital reverberation and apply them to produce a parametric audio effect that is capable of reproducing the main perceptual qualities of the spring reverberator while still allowing significant manipulation by the user.

This paper is organized as follows. In Section 1 we present the basic model for producing chirplike pulses, which appear in spring reverberation responses. Section 2 discusses further development of the model to include multiple echoes of the initial chirp and their progressive temporal blurring. Section 3 presents examples of fitting the model to responses recorded from different spring reverberation units. Section 4 concludes.

1 MODELING OF CHIRPS

We propose a model structure that produces responses similar to those observed in spring reverberation units. The simulation model is not physical, but is based on observations of characteristics present in recorded responses.

Fig. 1(a) shows an example response of a single spring. This spring is part of a reverberation tank taken from a Leem Pro KA-1210 guitar amplifier. This response was

*Manuscript received 2009 November 30; revised 2010 June 8.

measured using the sine sweep method [14]. The response lasts for several seconds, but we present only the first second. The sample rate used is $f_s = 44.1$ kHz, as in all examples of this paper. It is seen in Fig. 1(a) that the response contains a sequence of decaying pulses. The main pulse repeats at regular intervals of approximately 60 ms and becomes smeared over time while being attenuated.

To see better what is going on in the spring reverberation response, Fig. 1(b) shows the spectrogram of the signal in Fig. 1(a). The magnitude of a 512-point short-time Fourier transform (STFT) using the Blackman window with a hop size of 64 samples (that is, approximately 1.5 ms) is shown. In Fig. 1(b) we see that the response contains two sequences of dispersed pulses: the first one at low frequencies below about 4 kHz, which dominates the waveform in Fig. 1(a), and a second one best visible above 4 kHz, which is weaker and may extend through all frequencies, although only the first pulse is visible at low frequencies in Fig. 1(b). The maximum frequency of the first sequence of pulses is called the transition frequency f_C [15]. In this case we estimate $f_C = 4200$ Hz.

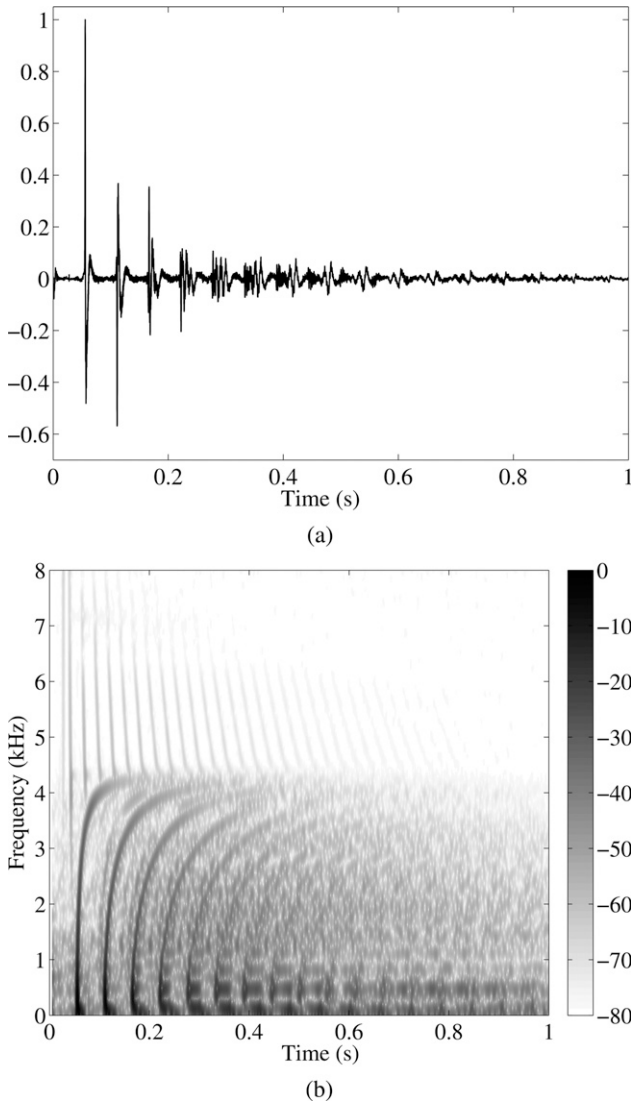

Fig. 1. Single spring response. (a) Waveform. (b) Spectrogram.

Fig. 2 shows another spectrogram where the beginning of the low-frequency chirp sequence is clearly visible. Now an 8192-point FFT is used with Blackman windows of 512 samples, and the linear magnitude (not dB) is displayed. The hop size is six samples to obtain a smooth spectrogram. The shape of the initial chirp and the next two echoes are clearly visible in Fig. 2. Next we will show how responses similar to this can be produced using a digital filter structure.

1.1 Interpolated Stretched All-Pass Filters

We have observed that a spectral delay filter [16] can produce a chirp similar in shape to those seen in Figs. 1(b) and 2. We have previously introduced the stretched all-pass filter as a generalization of the first-order all-pass filter [16]. The stretching is realized by replacing the unit delay in a first-order all-pass filter with a delay line of K samples, which yields the following transfer function:

$$A(z) = \frac{a_1 + z^{-K}}{1 + a_1 z^{-K}}. \tag{1}$$

As consequences of this operation, the impulse response becomes K times longer than originally, the filter's frequency response gets shrunk by the factor K with respect to frequency, and in addition, $K - 1$ image frequency responses turn up at high frequencies [16]. The stretched all-pass filter has the same structure as the Schroeder all-pass filter [5], which is also a first-order all-pass filter with an embedded delay line. The delay line of a stretched all-pass filter is usually short, typically between 2 and 20 samples, because the target is to produce a chirplike response by cascading many of these filters. In a Schroeder all-pass filter the delay line length is often hundreds or thousands of samples because it is used for artificial reverberation [17].

The transition frequency can be related to the stretching factor K by

$$f_C = \frac{f_s}{2K} = \frac{f_N}{K} \tag{2}$$

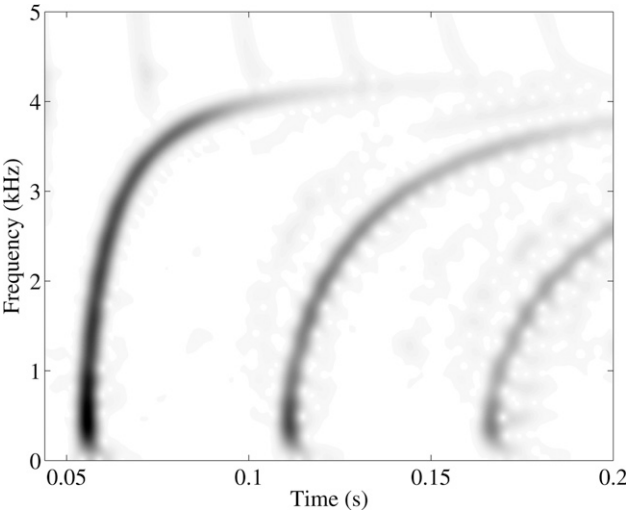

Fig. 2. Detail of spectrogram of single spring response in Fig. 1(b) obtained with different STFT parameters.

where f_s is the sampling frequency and $f_N = f_s/2$ is the Nyquist limit. Thus given a transition frequency f_C, the stretching factor K can be selected as

$$K = \frac{f_N}{f_C}. \tag{3}$$

For example, when the transition frequency is $f_C = 3.00$ kHz and the Nyquist limit is $f_N = 22.05$ kHz, the stretching factor will be $K = 7.35$. So to be able to produce a given transition frequency accurately it is necessary to implement also the decimal part of a fractional time delay. For this reason an interpolated delay line is needed in stretched all-pass filters in this application.

To implement delay-line interpolation we choose to use the first-order all-pass filter, which is easy to design to approximate a given fractional delay d [18]. The transfer function of the interpolated stretched all-pass filter then becomes

$$A_{low}(z) = \frac{a_1 + A_{fd}(z)z^{-K_1}}{1 + a_1 A_{fd}(z)z^{-K_1}} = \frac{a_1 + \frac{a_2 + z^{-1}}{1 + a_2 z^{-1}} z^{-K_1}}{1 + a_1 \frac{a_2 + z^{-1}}{1 + a_2 z^{-1}} z^{-K_1}} \tag{4}$$

where $K_1 = \text{round}(K) - 1$ is one less than the integral part of K and $A_{fd}(z) = (a_2 + z^{-1})/(1 + a_2 z^{-1})$ is the transfer function of the fractional delay all-pass filter. Fig. 3(a) shows a block diagram of the interpolated stretched all-pass filter. The proposed filter structure contains two nested all-pass filters. Nested all-pass filters have previously been used in artificial reverberation with much longer delay lines than in this work [10].

The coefficient a_1 in Eq. (4) adjusts the form of the group delay and hence the shape of the chirp [16] and a_2 determines the fractional delay [18], [19] so that

$$a_2 = \frac{1 - d}{1 + d} \tag{5}$$

where $d = K - K_1$ is one larger than the fractional (decimal) part of K. The range of delay parameter values is thus $0.5 \leq d < 1.5$.

Fig. 4 shows how chirps similar to those seen in Fig. 2 can be produced by cascading M identical interpolated stretched all-pass filters, such as is done to implement spectral delay filters [16]. Fig. 4(a) shows the spectrogram of the impulse response of a cascade of one hundred ($M = 100$) conventional first-order all-pass filters. The coefficient value of all filters is set to $a_1 = 0.75$, which is a useful value in practice. It is seen that a wide-band chirp is

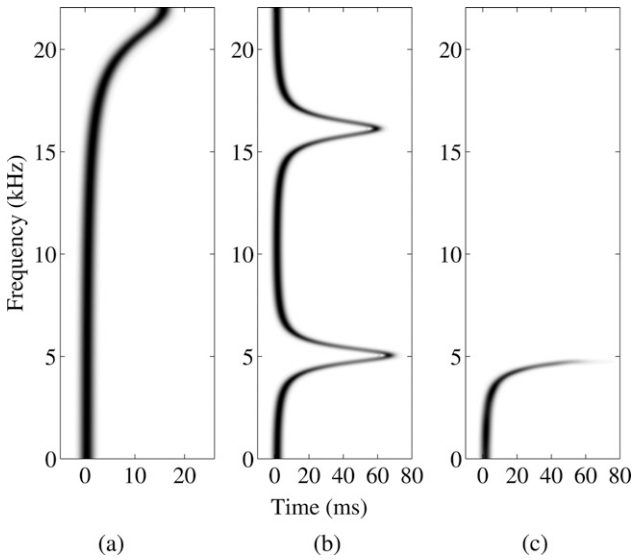

Fig. 4. Spectrograms. (a) Impulse response of 100 cascaded first-order all-pass filters ($K = 1$, $a_1 = 0.75$, $M = 100$). (b) Impulse response of 100 cascaded interpolated stretched all-pass filters ($K = 4.41$, $d = 1.41$, $a_1 = 0.75$, $M = 100$). (c) Low-pass filtered version of (b).

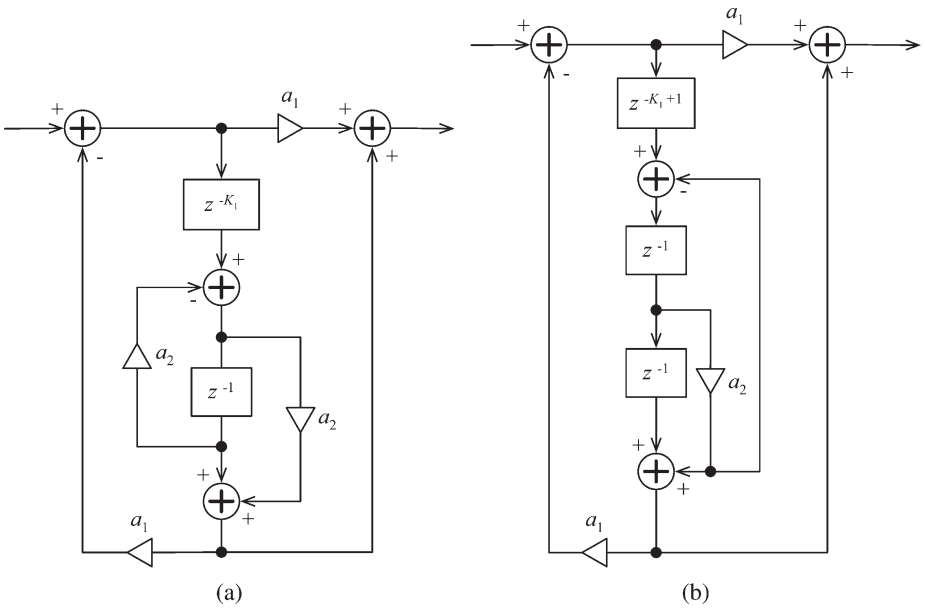

Fig. 3. (a) Block diagram of interpolated stretched all-pass filter consisting of two nested first-order filters. (b) Optimized version of (a) with one less multiplying coefficient.

produced that starts from 0 Hz and continues up to the Nyquist limit in about 16 ms.

Fig. 4(b) shows the spectrogram when a cascade of 100 interpolated stretched all-pass filters is used, and the stretching factor has been set to $K = 4.41$ in order to produce a transition frequency of 5 kHz. Every unit delay in the first-order all-pass filters has been replaced with a cascade of a delay line of three samples and a fractional delay all-pass filter approximating a delay of $d = 1.41$ sampling intervals, that is, $a_2 = -0.1701$ according to Eq. (5). In addition to a shrunk version of the original chirp (between 0 and 5 kHz), three image chirps appear. Notice that the length of the response is now K times longer than in Fig. 4(a), about 70 ms instead of about 16 ms. The image chirps can be suppressed by applying a low-pass filter at the output of the filter chain, which has been done to produce Fig. 4(c). A tenth-order elliptic IIR low-pass filter was used with a cutoff frequency of 4750 Hz, 1-dB passband ripple, and 60-dB stopband suppression. Although the parameters of this design example have not been calibrated to a recorded response, a comparison of Fig. 4(c) against Fig. 2 suggests that the proposed filter structure can produce good imitations of chirps that appear in responses of spring reverberation units. The parameterization is particularly simple because only three parameters are needed: all-pass filter coefficient a_1, number of filters in cascade M, and stretching factor K.

1.2 Optimizing the Low-Frequency Chirp Model Structure

It is possible to make several changes to the structure of the cascaded stretched all-pass filters which reduce the number of operations required per stage. First we can rewrite the first-order all-pass filter within the stretched all-pass filter structure in such a way as to allow the sharing of the coefficient multiplier block between both feedback and feedforward paths. This modification is possible at the cost of an extra unit delay [20]. This unit delay can be taken from the preceding large delay block, allowing a reduction of the operation count without any increase in memory requirements. Fig. 3(b) shows a single stretched all-pass filter optimized in this way.

An optimization of the cascaded stretched all-pass filters is possible by altering the order of operations to allow the sharing of a coefficient multiplier a_1 between the feedforward path of one section and the feedback path of the next section. Fig. 5(a) shows two cascaded stretched all-pass filter sections, whereas Fig. 5(b) shows two cascaded sections with the multiplier sharing implemented. When many identical stretched all-pass filters are cascaded, the sharing can only be implemented at the boundary of two neighboring filters. Therefore the first multiplier of the first section and the last multiplier of the last section cannot be shared with neighbors. The total number of multiplications is $2M + 1$ instead of the original $4M$, which corresponds to the cascading sections shown in Fig. 3(a). Hence in the case of large chains of cascaded stretched all-pass filters, these optimizations result in a reduction in multiplications of near 50%. However, the number of additions stays the same and the total saving in operations is instead near 25%.

1.3 Calibrating the Shape of the Low-Frequency Chirp Model

Fig. 6 presents an example of how well the first pulse can be imitated. Fig. 6(a) shows a pulse that has been extracted from a recording. Although pulses overlap in time in the original recording, it is possible to extract the complete pulse with some extra processing. An approximate model of the chirp must first be designed. It can be reversed in time to obtain an FIR filter response, which can be used for canceling the dispersion. The same idea has been suggested earlier by Abel et al. [3]. When the approximate chirp is sufficiently accurate, the filtering turns the first chirp into a short pulse, which is separated in time from other chirps, and it can then be easily separated from the long signal. This is how the pulse in Fig. 6(a) was obtained.

Fig. 6(b) shows a synthetic pulse produced using interpolated stretched all-pass filters. The estimated parameters in this case are $f_c = 4.2$ kHz, $a_1 = 0.62$, and $M = 100$. The choice of the transition frequency f_c leads to $K = 5.25$.

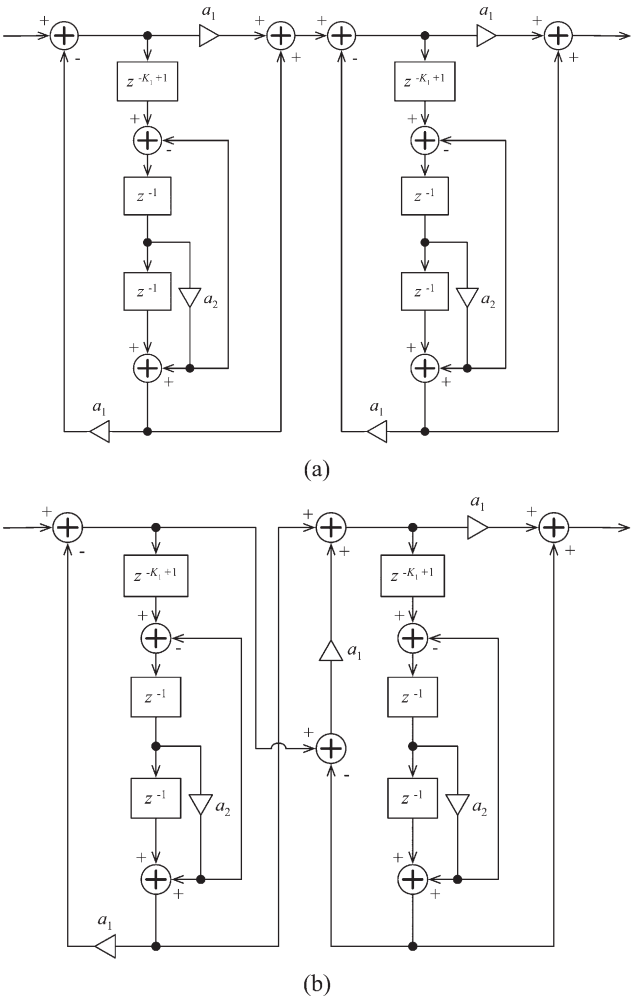

Fig. 5. (a) Two cascaded interpolated stretched all-pass filters with identical filter coefficients. (b) Filters in (a) sharing a multiplying coefficient.

We get a stroke of luck because a very good match is achieved, although we have few degrees of freedom to adjust the shape of the synthetic pulse. The largest deviation between the original and the synthetic pulse appears around 4 kHz. Perceptually the two short chirps sound identical, however.

Fig. 7 shows the spectra of the first two prominent chirps that appear in the recorded response. These chirps begin at about 0.055 and 0.110 s in Fig. 2. The two spectra have been computed with the 16 384-point FFT from 20- and 40-ms-long straightened chirps, respectively. Spectral smoothing has not been applied. The spectrum of the first chirp is very smooth whereas the second one contains ripple. Both spectra have a very similar overall shape. They peak at about 100 Hz with lower frequencies much suppressed and an approximately −8 to −10 dB per octave slope toward higher frequencies. Above 4 kHz the spectra decay quickly because the low-frequency chirps fade away as they reach the transition frequency, as seen in Fig. 1(b).

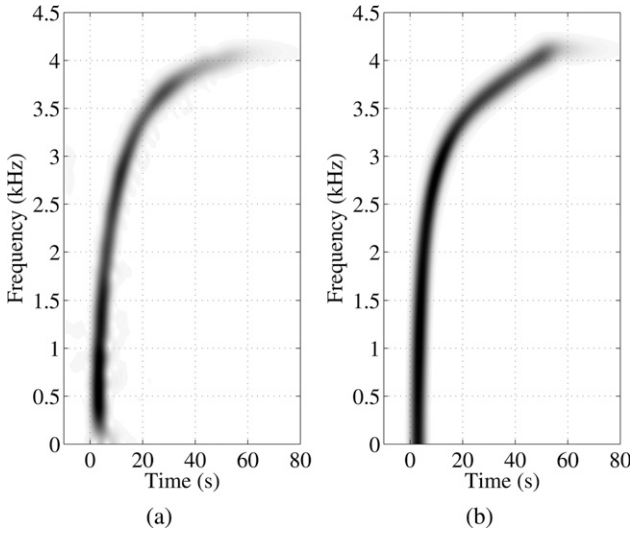

Fig. 6. (a) Extracted first chirp of recorded spring reverberation response. (b) Imitation of (a) produced with interpolated stretched all-pass filters. Cutoff frequency of low-pass filter is 98% of transition frequency (4200 Hz).

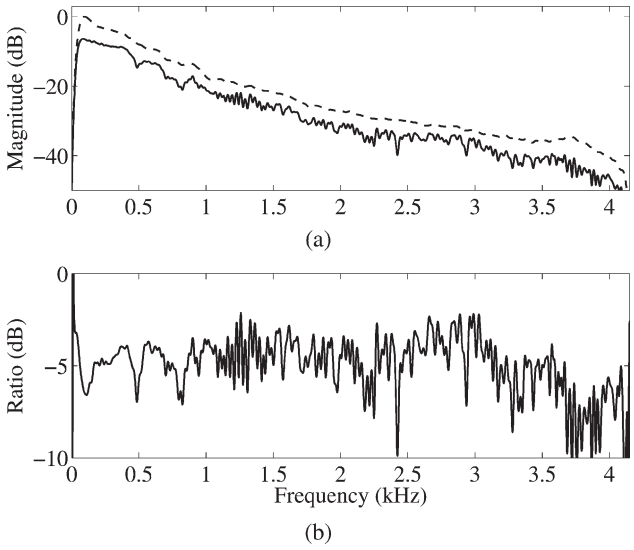

Fig. 7. (a) Spectra of first and second prominent chirps in measured response. (b) Their ratio.

Fig. 7(b) shows the ratio of the chirp spectra, which can be interpreted as the magnitude response of the filter that converts the first signal to be the second one. It is evident that a complicated filter would be needed to do this accurately. However, in a simplified model we may discard the details and just measure the overall attenuation, which is about −4.5 dB between 1 and 3 kHz. We see from Fig. 1(a) that the polarity of the second pulse appears to be inverted with respect to the first. A gain coefficient of −0.60 thus is a simple approximation to what happens to the pulse amplitude as it travels one roundtrip back and forth in the spring.

1.4 Equalizing the First Chirp

We have manually designed a low-order equalizing filter that approximates the spectral shape of the first chirp and that can be applied to the output signal of the spring reverberation algorithm. We have decided to use a second-order IIR filter with zeros at 0 Hz and at the Nyquist limit [21], [22], which we stretch by replacing each unit delay by a sequence of K_{eq} unit delays to obtain enough suppression around the transition frequency,

$$H_{eq}(z) = \frac{A_0}{2}\frac{1 - z^{-2K_{eq}}}{1 + a_{eq1}z^{-K_{eq}} + a_{eq2}z^{-2K_{eq}}} \tag{6}$$

where $a_{eq1} = -2R\cos\theta$, $a_{eq2} = R^2$, the cos θ term sets the pole angle, R is the pole radius, and the scaling factor A_0 that sets the peak gain to 0 dB is defined as $A_0 = 1 - R^2$. The cos θ term can be computed from the desired peak frequency f_{peak} in the following way [22]:

$$\cos\theta = \frac{1 + R^2}{2R}\cos\left(\frac{2\pi f_{peak}K_{eq}}{f_s}\right). \tag{7}$$

Fig. 8 compares the spectra of the first chirp and the impulse response of the filter in Eq. (6), when we have chosen a peak frequency f_{peak} of 95 Hz and a −3-dB bandwidth of 130 Hz. We obtain the pole radius R from the bandwidth in the following way:

$$R = 1 - \frac{\pi B K_{eq}}{f_s}. \tag{8}$$

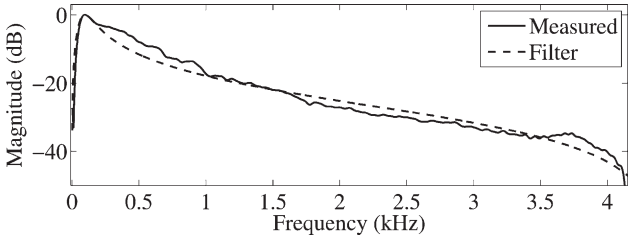

Fig. 8. Spectrum of first chirp and magnitude response of parametric equalizing filter $H_{eq}(z)$.

In Eq. (6) it is convenient to choose an integer delay line length K_{eq}, and since the signal above the transition frequency will be suppressed, we may choose any number smaller than K; for example, $K_{eq} = \text{floor}(K)$. This implies that the frequency response of the equalizing filter will have image responses at frequencies above $f_s/[2\text{floor}(K)]$. In this example we have $K_{eq} = 5$, so the image responses appear above 4410 Hz, and they will be discarded by a low-pass filter. It is seen in Fig. 8 that the resonator with zeros matches the measured spectrum of the first chirp very well around the peak at 95 Hz, and the overall spectral slope is approximately right, although the filter's magnitude response is about 5 dB too small around 500 Hz and a few dB too large between 1.7 and 3 kHz.

1.5 Modeling the High-Frequency Chirps

In order to model the high-frequency chirps visible above 4 kHz in Fig. 1(b), we can also apply a spectral delay filter. The shape of this high-frequency chirp is simpler than that observed for the low-frequency chirps. The first frequencies to arrive are at the Nyquist limit and the last frequencies to arrive are toward dc (that is, 0 Hz). We can therefore approximate the shape of this chirp by cascading a number of first-order all-pass filters with a suitably chosen negative coefficient. The transfer function of the spectral delay filter is thus

$$A_{\text{high}}^{M}(z) = \left(\frac{a_{\text{high}} + z^{-1}}{1 + a_{\text{high}} z^{-1}} \right)^{M}. \tag{9}$$

We need the filter to be dispersive over a relatively wide range of frequencies, with the maximum group delay occurring near dc. Therefore we choose a negative coefficient value, such as $a_{\text{high}} = -0.6$. A single section of this filter structure does not produce as much group delay as a stretched all-pass filter, due to both the lower coefficient value and the lack of stretching effect. It is therefore necessary to choose a higher value of M to produce the desired chirp length. A value of M double that chosen for the low-frequency chirps proves to be appropriate audibly. The extra computational cost of cascading more filter stages is offset somewhat by the fact that each filter is a first-order section and hence requires approximately half the operations per stage required by the interpolated stretched all-pass filter.

The optimization for cascaded all-pass sections with identical coefficients discussed in Section 1.2 can also be applied to the cascaded first-order sections used here. In the limit, as the size of the cascaded all-pass chain increases, the saving in operations approaches 25%.

2 SYNTHESIS OF CHIRP SEQUENCES

In this section we propose two feedback structures to produce decaying chirp sequences. A modulation technique is introduced to reproduce the temporal blurring noted in the impulse responses, which brings about a reverberant quality in the chirp sequences.

2.1 Low-Frequency Feedback Delay Structure

We denote the proposed feedback structure for modeling the chirp sequence below the transition frequency by C_{lf}, where "lf" refers to low frequency. It contains a cascade of many all-pass filters, a long delay line, a loop gain coefficient, and a dc blocking filter $H_{\text{dc}}(z)$ in a feedback loop. The long delay line uses multiple output taps and is modulated using a random signal, which will be discussed in Section 2.3. In addition the output signal of the feedback loop is processed with an equalization filter as discussed in Section 1.4 and a low-pass filter. The structure is shown in Fig. 9. Feedback structures containing a spectral delay filter have been studied previously by Pekonen et al. [23].

The delay line length can be calculated based on the delay time T_{D} of the spring unit and the group delay of the all-pass filter chain. The delay time T_{D} can be estimated from the spectrogram of the recorded impulse response as the period of pulses at low frequencies. The delay line length L is then obtained by subtracting the contribution of the all-pass filter chain's group delay at dc from the delay time in samples, that is,

$$L = T_{\text{D}} f_s - \tau_g(0) \tag{10}$$

where the group delay of the interpolated stretched all-pass filter chain at dc is

$$\tau_g(0) = KM \frac{1 - a_1}{1 + a_1}. \tag{11}$$

In our example case of Fig. 1, the time delay is estimated to be $T_{\text{D}} = 56$ ms, or 2470 samples, and the group delay of

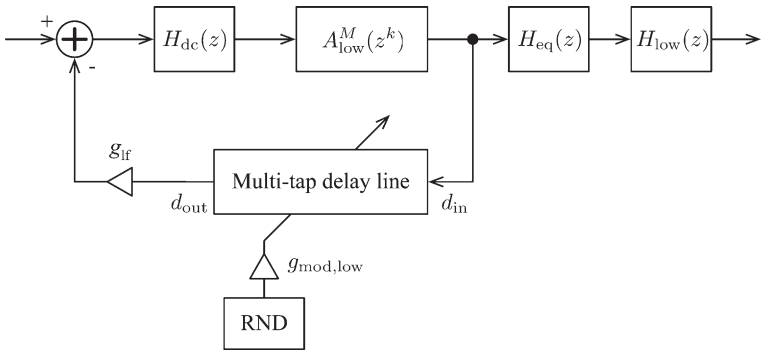

Fig. 9. Block diagram of feedback structure C_{lf} used to produce the sequence of progressively blurred chirps beneath the transition frequency.

the all-pass filter chain with $a_1 = 0.62$, $K = 5.13$, and $M = 100$ is 120 samples at dc. According to Eq. (10) the delay line length is estimated to be $L = 2350$ samples, or about 53 ms.

Note that this simple structure neglects the fact that, in the recorded signal, the second pulse has actually three times the dispersion characteristics of the first pulse, the third pulse five times and so on. In this simplified model the second pulse has traveled though the dispersion filter only twice, the third pulse three times, and so on. As the dispersion characteristic of the first arrival is accurate, we expect that this simplification is not perceptually significant.

The measured spring responses appear to lack low frequencies near dc. The chirp sequences also show an increased delay at very low frequencies, which is observed as a smearing effect at the foot of each chirp in Fig. 1(b). To implement these effects with the feedback delay structure, a dc blocker is inserted in the feedback loop. We choose the following transfer function:

$$H_{\mathrm{dc}}(z) = \frac{1 + a_{\mathrm{dc}}}{2} \frac{1 - z^{-1}}{1 - a_{\mathrm{dc}} z^{-1}} \tag{12}$$

where $(1 + a_{\mathrm{dc}})/2$ is a scaling factor to ensure a maximum gain of 0 dB, and the coefficient a_{dc} depends on the −3-dB frequency f_{cutoff} in the following way:

$$a_{\mathrm{dc}} = \tan\left(\frac{\pi}{4} - \frac{\pi f_{\mathrm{cutoff}}}{f_{\mathrm{s}}}\right). \tag{13}$$

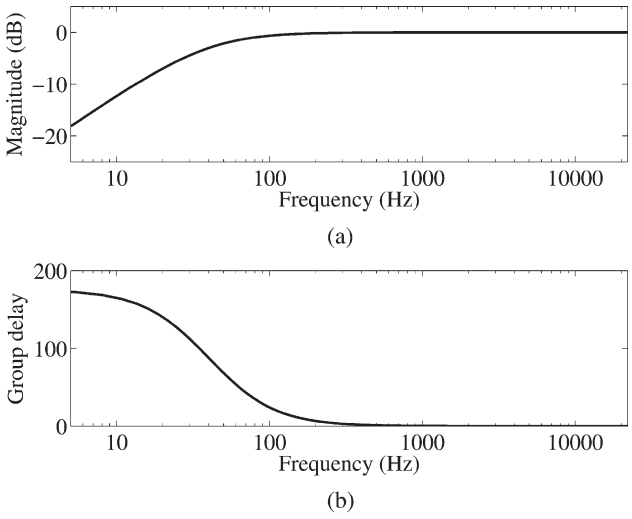

Fig. 10. Properties of dc blocking filter $H_{\mathrm{dc}}(z)$. (a) Magnitude response. (b) Group delay. Sampling rate 44.1 kHz.

The derivation of Eq. (13) has been presented in [24].

By setting $f_{\mathrm{cutoff}} = 40$ Hz in Eq. (13), when $f_{\mathrm{s}} = 44.1$ kHz, the filter coefficient becomes $a_{\mathrm{dc}} = 0.9943$. The magnitude response and the group delay of the resulting dc blocking filter are displayed in Fig. 10. It is seen in Fig. 10(a) that very low frequencies are well attenuated but the magnitude response is 0 dB (within 1 dB) above 100 Hz. Fig. 10(b) also shows that the filter introduces a large delay at very low frequencies, about 87 samples (that is, 2.0 ms) at 40 Hz. These are the desired properties for the spring reverberation algorithm.

2.2 Multiple Delay Line Taps

The delay line in the feedback path of the structure C_{lf} can be augmented to reproduce other features seen in Fig. 2 at little extra computational cost. This is accomplished by introducing additional output taps at a number of places along the delay line. This can alternatively be thought of as splitting the delay line into several separate sections, with feedforward paths bypassing each. Fig. 11 shows this structure explicitly. We apply this technique only to the low-frequency chirp sequence model.

Varying the length of the delay line skipped by these feedforward paths allows us to produce a number of effects. Allowing some amount of the signal to skip ahead a small amount of samples in the delay line produces the equivalent of a comb filter within the feedback path of the structure. This property has been used previously to introduce frequency-dependent variations into the loop gain of another feedback system, a waveguide string model [25], with the spacing of the variations dependent on the length of the delay line portion skipped. This technique is known as a ripple filter. If we connect the ripple filter length L_{ripple} to the value of K used for the stretched all-pass filter,

$$L_{\mathrm{ripple}} = 2KN_{\mathrm{ripple}} \tag{14}$$

we gain the parameter N_{ripple}, which allows us to specify the number of ripples in the loop gain below the transition frequency. By appropriate choice of values for N_{ripple} and the ripple filter coefficient g_{ripple} we can produce a variety of different frequency-dependent reverberation time characteristics. An example of this could include biasing the reverberation time toward the lower half of the band beneath the transition frequency by setting $N_{\mathrm{ripple}} = 0.5$ and choosing a positive value of g_{ripple}, such as $g_{\mathrm{ripple}} = 0.1$. Alternatively, by choosing a higher value of N_{ripple} we can introduce multiple bands in which the reverberation

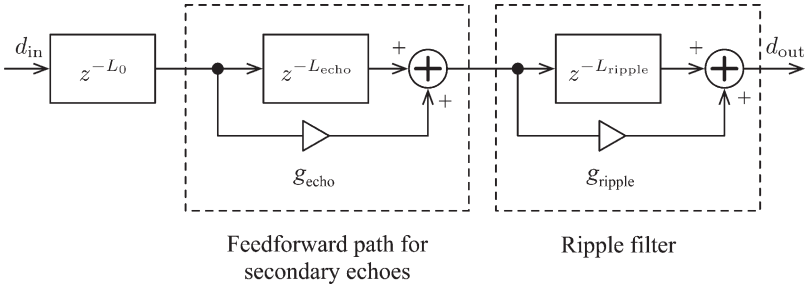

Fig. 11. Block diagram of internal structure of multitap delay line used in low-frequency chirp feedback delay structure.

time is longest. An example of such behavior is shown in Fig. 12.

In Fig. 1(b) faint "preechoes" can be seen preceding each of the main echoes below the transition frequency. These preechoes can be derived via examination of the dispersion relation of a continuous model of spring vibration [15]. This feature can be replicated by introducing a feedforward path, which skips a relatively large part of the delay line. Measured spring responses show that this preecho arrives around 10 ms before the main echo, when then main echoes are spaced by around 50 ms. Analysis of the continuous model predicts approximately the same relationship. We therefore construct a feedforward path that bypasses one-fifth of the delay line. We set the length of this section of the delay line to be $L_{\text{echo}} = L/5$. From Fig. 1(b) we can measure that the preechoes are approximately 20 dB lower in amplitude than the main echoes. Therefore we choose the feedforward coefficient for this section $g_{\text{echo}} = 0.1$. The remaining delay line length L_0 can be calculated from the lengths of the subsections discussed previously and the total delay line length desired,

$$L_0 = L - L_{\text{echo}} - L_{\text{ripple}}. \tag{15}$$

Fig. 13 shows the effect that the addition of the echo path has on the response of the system. It is seen that each chirp after the first has one or more preechoes. The preechoes become more numerous as the signal circulates in the feedback loop.

The dc blocking filter is also used in the simulation for Fig. 13. Its effects are seen as the fast decay of very low frequencies and as the smearing of the feet of the chirps near dc.

2.3 Delay Line Modulation

As can be seen from Fig. 1(b), each successive echo produced by the spring becomes more diffuse and blurred, lending the sound its reverberant quality. This property could be modeled by inserting a digital reverberator into our feedback structure. Instead we take the simpler approach of modulating the length of the main delay line with a filtered noise signal. Linear interpolation is used to produce fractional delay line lengths [26]. This process produces a gradual blurring and spreading of the individual chirps, in both the time and frequency domains, which sounds reverberant. Random modulation of delay line lengths within the structure of a digital reverberator is a known technique [27], [28]. It is usually used to break up resonances within the structure and to reduce any repeating, metallic, or static quality in the tail of the reverberations. We take the process further and use it as the main mechanism for progressive decorrelation of sound within the structure.

We choose the noise signal based on two criteria. First the value of the signal must be strictly bounded for reasons of implementation. A uniform random distribution fulfills this criterion and therefore presents a good starting point. Second, to maintain some kind of physical analogy, the noise signal should have roughly a $1/f$ spectrum. We can achieve this by filtering our uniformly distributed random number sequence, namely, white noise, with a normalized leaky integrator of the form

$$H_{\text{int}}(z) = \frac{1 - a_{\text{int}}}{1 - a_{\text{int}} z^{-1}}. \tag{16}$$

We set $a_{\text{int}} = 0.93$. This produces a filter response that is flat up to around 100 Hz and which decreases with $1/f$ above 100 Hz. The noise signal filtered with Eq. (16) has an approximately normal (Gaussian) distribution and its variance is proportional to the original random signal's variance divided by the term $1 - a_{\text{int}}^2$ (see, for example, [29]),

$$\sigma_{\text{nf}}^2 = \frac{(1 - a_{\text{int}})^2}{1 - a_{\text{int}}^2} \sigma_n^2 \tag{17}$$

where $\sigma_n^2 = 0.3333$ is the variance of the original random number sequence and $(1 - a_{\text{int}})^2$ is the scaling coefficient for signal power based on the numerator of Eq. (16). When we choose $a_{\text{int}} = 0.93$, the variance σ_{nf}^2 of the

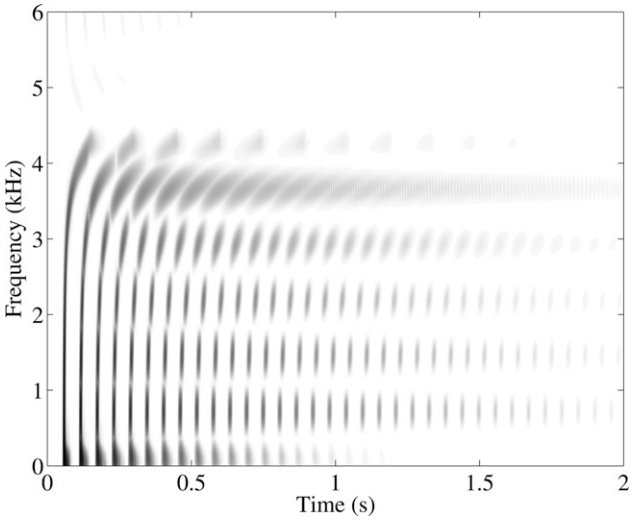

Fig. 12. Spectrogram of impulse response of C_{lf} with ripple filter feedforward path added.

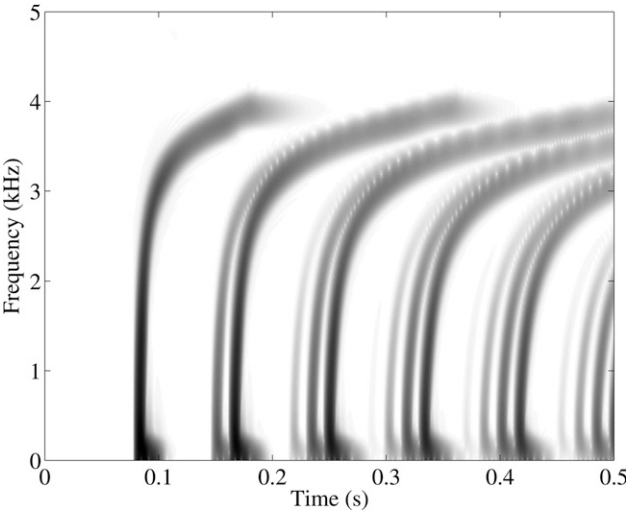

Fig. 13. Spectrogram of impulse response of C_{lf} with preecho feedforward path and dc blocking filter added.

filtered noise signal becomes 0.0121. The corresponding standard deviation is $\sigma_{nf} = 0.101$, so 99% of the sample values will stay within $\pm 3\sigma_{nf}$, but will often exceed it at audio rate. Fig. 14 shows an example of a filtered noise sequence. We may safely assume that the noise signal samples lie within the interval $[-1, 1]$ and use hard clipping if they exceed it, without spoiling the modulation technique. We can then multiply the noise signal by our desired modulation depth g_{mod} in samples. Varying this modulation depth also varies the rate at which the system descends into its reverberant tail, and therefore it is a useful parameter to leave adjustable for the user. Modulation depths on the order of around 30 samples or less produce pleasing results. An example of the progressive blurring effect produced by this modulation on a chirp sequence is given in Fig. 15.

2.4 High-Frequency Feedback Delay Structure

We may similarly produce a structure to replicate the high-frequency pulses seen in Fig. 1(b). We denote this structure by C_{hf}, and it can be seen in Fig. 16. Fig. 17 shows the spectrogram of the impulse response of this structure with example parameters. The chirps modeled by this structure are present at a significantly lower level in the impulse response of a real spring [see Fig. 1(b)] and therefore are less perceptually important. Hence we do not attempt to match the frequency profile from the measured response, and omit the equalizing filters used in C_{lf}. The delay line length in C_{hf} should be set relative to the delay line length in C_{lf}. Examination of Fig. 1(b) reveals that the high-frequency chirps repeat at around three times the rate of low-frequency chirps. Ideally, in order to prevent any repetitive elements or patterns in the decay portion of the reverberation structure, the ratio between L and L_{high} should be mutually prime. In practice it is sufficient to choose, for example, $L_{high} = L/2.3$, as this will produce repetition only over a long enough time scale to be inaudible. This ratio is a function of the helical angle of the spring, and it will be in this range for most commercial spring reverberators.

The effect of the delay line modulation is stronger at higher frequencies. It blurs high frequencies faster than low frequencies, and also it causes some slow damping of high frequencies due to linear interpolation of the delay line. To avoid reducing the overall decay time of the system too greatly, we increase the feedback loop gain from the value estimated in Section 1.3. To compensate for the faster blurring of high frequencies, we empirically set a lower modulation depth $g_{mod,\,high}$ for the noise signal used within C_{hf}, of half that used in C_{lf}.

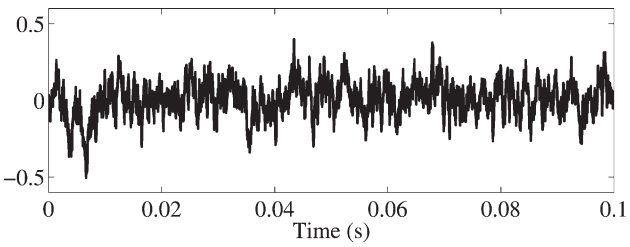

Fig. 14. Example of using filtered random numbers for modulating feedback delay line.

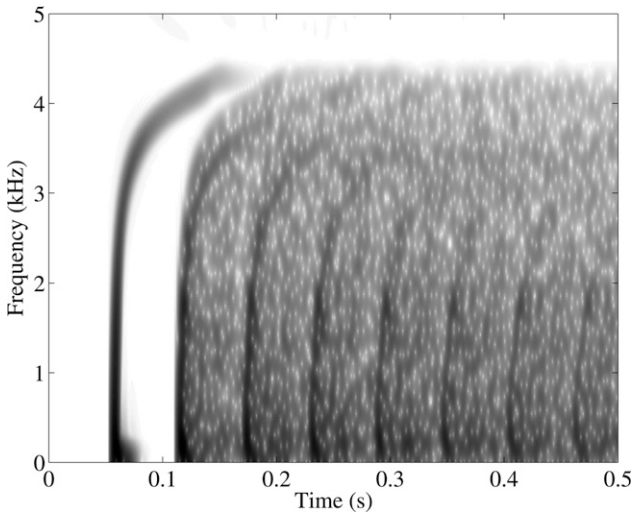

Fig. 15. Spectrogram of impulse response of C_{lf} with random delay line length modulation added to feedback path.

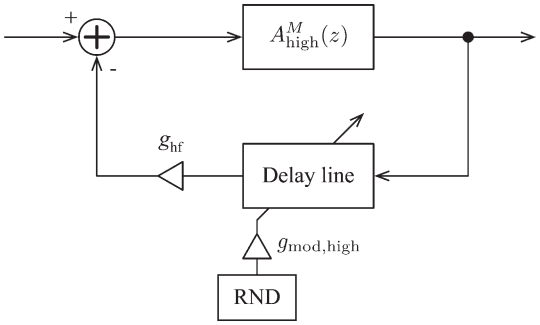

Fig. 16. Block diagram of feedback structure C_{hf} used to produce the sequence of progressively blurred chirps above the transition frequency.

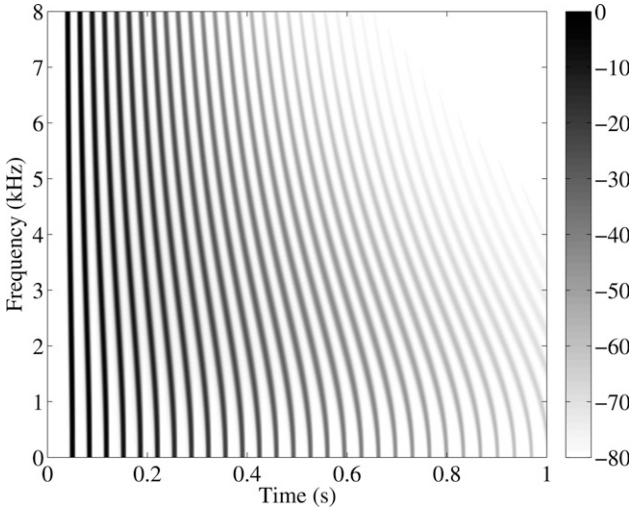

Fig. 17. Spectrogram of a synthetic pulse sequence produced using structure of Fig. 14 with parameters $a_1 = -0.6$, $M = 200$, $L = 900$, and $g_{hf} = -0.77$. Random modulation is turned off.

2.5 Combining and Coupling the Chirp Sequence Structures

We have now developed two structures, C_{lf} and C_{hf}, which model the main features visible in the impulse response of a spring. These models must then be combined to produce a complete spring model. This is done by placing the two models in parallel, with the addition of a processing-free path to carry the "dry" signal. Models of spring reverberation show that these modes are coupled [4], [5], [15]. We couple C_{lf} and C_{hf} by adding crossed feedback paths between them, controlled by coupling coefficients c_1 and c_2. The combined structure is shown in Fig. 18.

Increasing the coupling coefficients c_1 and c_2 results in interaction between the two feedback structures, and hence a more complex response. Care must be taken when increasing c_2, the coefficient governing the amount of signal fed from the output of C_{lf} to the input of C_{hf}, as the faint image chirps of the stretched all-pass filter in C_{lf} can interact with the high-frequency chirps of C_{hf} and produce unwanted high-frequency content. This can be rectified by increasing the order of the low-pass filter in C_{lf}, but at the cost of greater computational cost and problems with the low-pass filter ringing at its cutoff frequency. Increasing the coupling coefficient c_1 produces no such problem, and may happily be used with small values, such as $c_1 = 0.1$, to increase the complexity of the reverberant tail of the combined system.

Measurements taken from the spectrogram in Fig. 1(b) show that the high-frequency chirp sequence is around 60 dB quieter than the low-frequency chirp sequence, and therefore we suggest that the relative output gains o_{low} and o_{high} of the two chirp sequence models be set to reflect this. This can be achieved by setting the constraint that $o_{\mathrm{high}} = o_{\mathrm{low}}/1000$. The relative values of o_{low} and o_{dry} are application dependent and are intended to be set appropriately by the final user.

2.6 Physically Informed Model Parameterization

We can make a number of further alterations to the parameterization of our model. First we can use results derived from a continuous model of spring vibration [15] to link our model parameters f_{C} and T_{D} with measured geometrical properties of a particular spring. These relationships are given as

$$T_{\mathrm{D}} \approx \frac{4L_{\mathrm{wire}}R_{\mathrm{helix}}}{r\sqrt{E/\rho}} \tag{18}$$

and

$$F_{\mathrm{C}} \approx \frac{3r\sqrt{E/\rho}}{16R_{\mathrm{helix}}^2\sqrt{5\pi}} \tag{19}$$

where L_{wire} is the uncurled length of the wire, R_{helix} is the radius of the helix, r is the radius of the wire, ρ is the density of the materials, and E is Young's modulus of the material. This allows an alternative parameterization of the model, which may be advantageous in situations where physical measurements of a spring are more easily obtained than measurements of its response or when tuning the model via more intuitive physical parameters is desired.

It can also be observed by inspection of a number of spring responses that the effective length of each individual low-frequency chirp is around 50% greater that the delay time T_{D} of a particular spring. This can be accounted for in the parameter model by linking the number M of cascaded all-pass sections in C_{lf} with the value of T_{D},

$$M = \frac{3}{2}\frac{T_{\mathrm{D}}}{K\delta_{99.9}} \tag{20}$$

where $\delta_{99.9}$ is the duration of the impulse response of a first-order all-pass filter that contains 99.9% of its total energy [16], [30].

3 APPLICATION EXAMPLES

3.1 Modeling a Single Spring

Fig. 19 shows the result of trying to match the spring response shown in Fig. 1 with the model described in the preceding. Internal parameters of the chirp sequence models are set as described in Sections 1 and 2. The values of the more general parameters T_{D} (delay time) and f_{C}

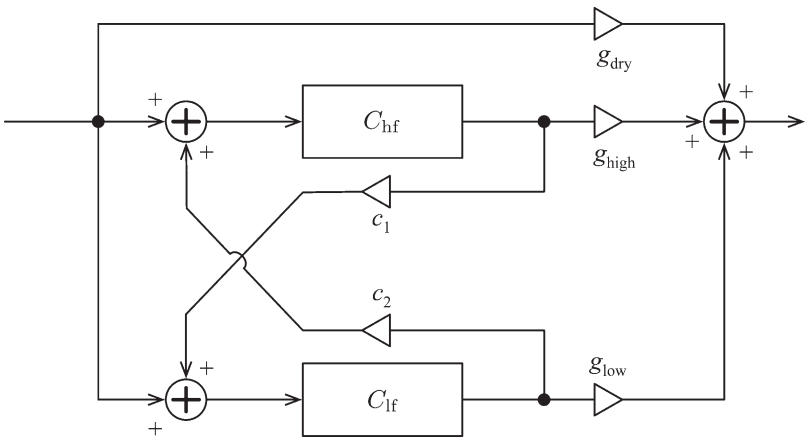

Fig. 18. Block diagram of structure of complete spring model, including low-frequency and high-frequency chirp sequence models and their coupling.

(transition frequency) are set to match the values measured from the impulse response in the spring. Fig. 20 shows the response of a different spring taken from the Leem Pro KA-1210 reverberation unit and an attempt to match it using the spring model. Table 1 lists the values of the parameters used with the model to produce these responses.

Inspection of the spectrograms in Figs. 19 and 20(b) shows that the broad properties of spring responses are modeled well. The spectrograms also reveal some minor differences; for example, the exact chirp shape is not recreated, but the importance of this perceptually is arguable. The progressive temporal blurring of the pulses appears more regular in the model than in the real spring response, as might be expected. From a subjective, perceptual perspective, the sound of the model seems to possess both spring like and reverberant qualities. Compared with a real unit, the later more diffuse section of the reverberative tail sounds rather less colored. No serious attempt has been made to model the complex modal structure of the real spring, so this is expected. Some improvement could perhaps be achieved in this area by adding a number of extra ripple filters to the multitap delay line of C_{lf} in order to produce a more complex variation of reverberation time with frequency.

Fig. 21 shows the spectrogram of the impulse response of the spring model when set to a high T_D value of 0.2 s, but a low f_C value of 2000 Hz. Such a configuration would be unusual in a real spring reverberation unit. The impulse response sounds similar to a standard spring response, but somehow darker and more spacious. This illustrates the potential of a parametric model to produce results that are related to the modeled real unit, but exaggerated or warped in potentially interesting ways.

The spring reverberation algorithm has been tested by applying it to various musical instrument sounds. To give

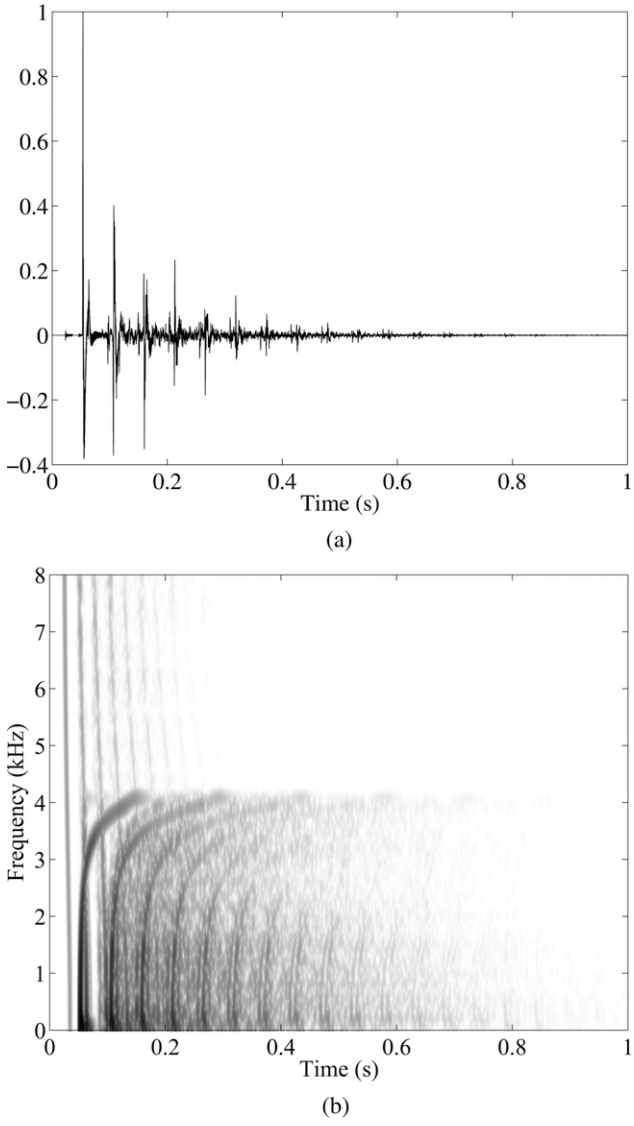

Fig. 19. Impulse response of spring model, with parameters tuned to mimic spring response of Fig. 1. (a) Waveform. (b) Spectrogram.

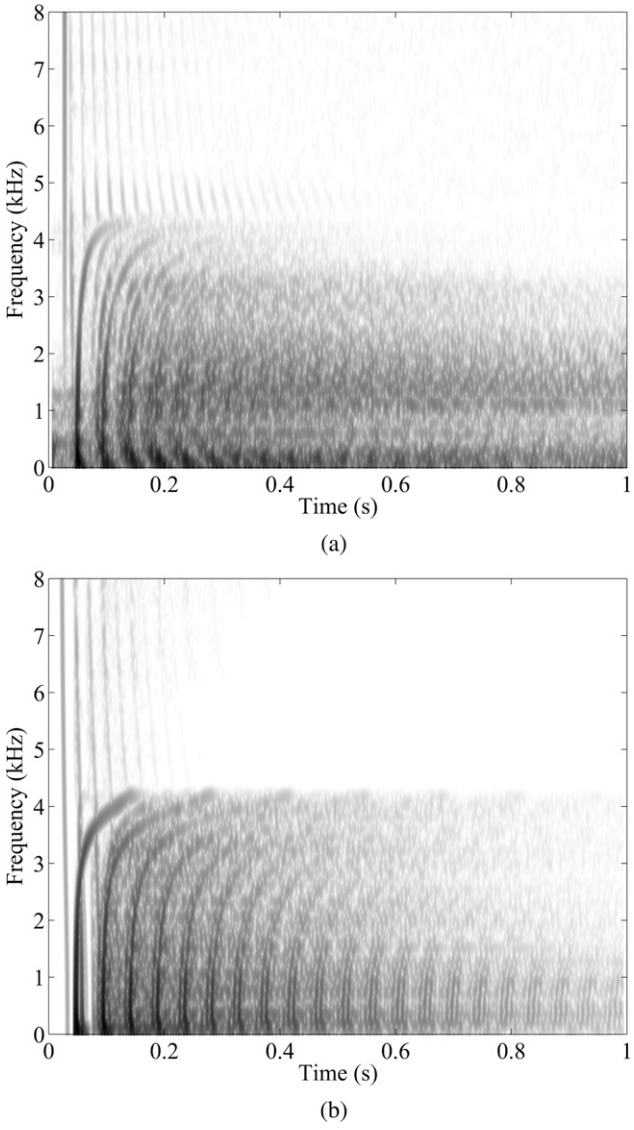

Fig. 20. Spectrograms. (a) Real spring taken from unit in Fig. 1. (b) Spring model with parameters tuned to mimic spring response (a).

an example, Fig. 22(a) shows the spectrum of a synthesized musical phrase, an arpeggio, created using an FM synthesizer, and Fig. 22(b) shows this arpeggio processed with a single spring model of parameters similar to those discussed. Listening to this processed phrase, the model spring sounds very much like a real spring reverberation unit. The complex nature of the input signal hides the flaws of the model that were audible in the impulse response.

Table 1. Parameter values used for simulating the springs examined.*

	Leem Pro KA-1210			Sansui RA-700
	Spring 1	Spring 2	Spring 3	Spring 1
T_D	0.056	0.044	0.047	0.056
f_C	4300	4400	4450	3526
M_{high}	200	200	200	200
M_{low}	100	100	100	100
g_{lf}	−0.8	−0.8	−0.8	−0.8
g_{hf}	−0.77	−0.77	−0.77	−0.77
g_{high}	0.001	0.001	0.001	0.001
g_{mod}	8	12	10	6
C_1	0.1	0.1	0.1	0.2
C_2	0	0	0	0
N_{ripple}	0.5	0.5	0.5	0.5
g_{ripple}	0.1	0.1	0.1	−0.2
g_{echo}	0.1	0.1	0.1	0.1

*Two different spring reverberation units are simulated. The Leem Pro KA-120 is a unit that utilizes three springs in parallel. Of these, spring 1 corresponds to the simulation of the spring presented in Fig. 1, and spring 2 to the one presented in Fig. 20(a). Spring 3 is the third spring from the unit. The second unit examined is the Sansui RA-700, which contains only one spring. Spectrograms of the real and simulated RA-700 springs are presented in Fig. 25.

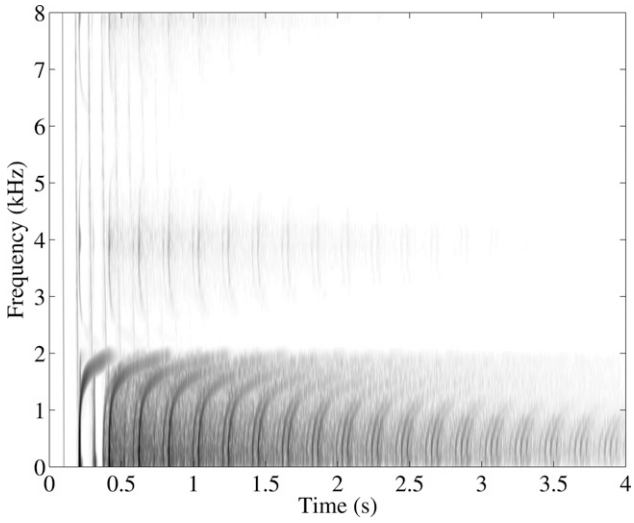

Fig. 21. Spectrogram of impulse response of spring model set to long T_D and low f_C.

3.2 Modeling a Complete Spring Reverberation Unit

Many real spring reverberation units employ a number of springs of slightly different geometric properties, connected in parallel. The purpose of the configuration is to generate a denser pattern of echoes. We can reproduce this configuration simply by connecting several spring models in parallel. The structure of such a configuration is shown in Fig. 23.

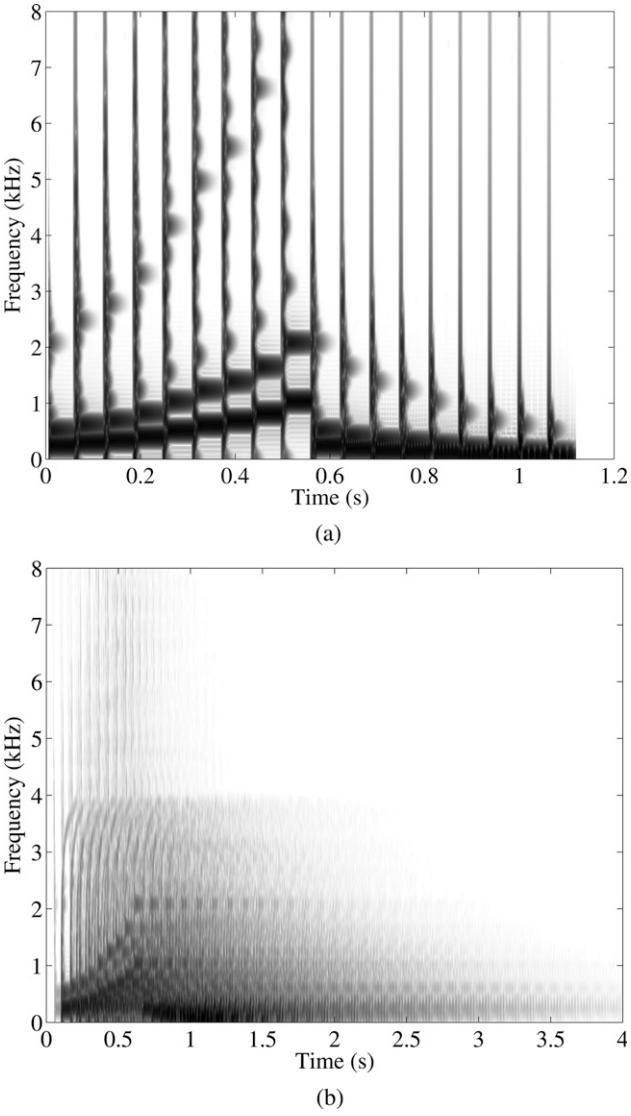

Fig. 22. Spectrograms (a) Test arpeggio generated with FM synthesis. (b) Same signal treated by a single spring model. Note different time scales in (a) and (b).

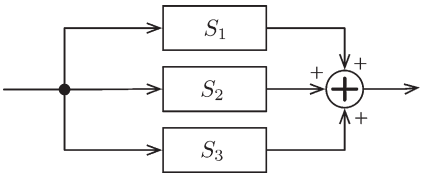

Fig. 23. Block diagram of three spring models placed in parallel, hence forming a model of a simple three-spring reverberation unit.

The Leem Pro KA-1210 reverberation unit consists of three springs in parallel, two of which we have attempted to model in Section 3.1. The response of the unit as a whole is shown in Fig. 24(a). We can combine these two models with a third spring model in an attempt to model the unit as a whole. The result of this is shown in Fig. 24(b). Table 1 lists the parameter values used with the three spring models to produce this response. The same similarities and inaccuracies discussed in Section 3.1 with respect to single springs are obviously present in the three-spring model, and the audible effect is much the same. This shows that several parametric spring reverberation models can be combined in the same fashion as in real spring reverberation units to enrich their response.

3.3 Modeling Another Spring Reverberation Unit

Some spring reverberation units employ only a single spring. An example of such a unit is the Sansui RA-700, a unit intended to be used as part of a home audio setup. Fig. 25(a) shows the measured impulse responses of the Sansui unit. It appears similar to the single-spring impulse responses examined previously, with the notable exception that high-frequency components of both the low and high chirp sequences are much more prominent. It also appears that in contrast to the other responses examined, this response decays slowest at a point near the top of the lower chirp sequence, rather than at low frequency. This characteristic can be reproduced by using the ripple filter section of the C_{lf} structure.

Fig. 25(b) shows an attempt to model this response, using the parameters given in Table 1. Note that this model response has been differentiated, as a crude attempt to match the overall spectral tilt of the response. The different spectral profile of this unit implies that it might be wise to further develop the equalizing resonator $H_{\mathrm{eq}}(z)$ used as part of the C_{lf} model to allow parametric variations of the strength and direction of the spectral tilt

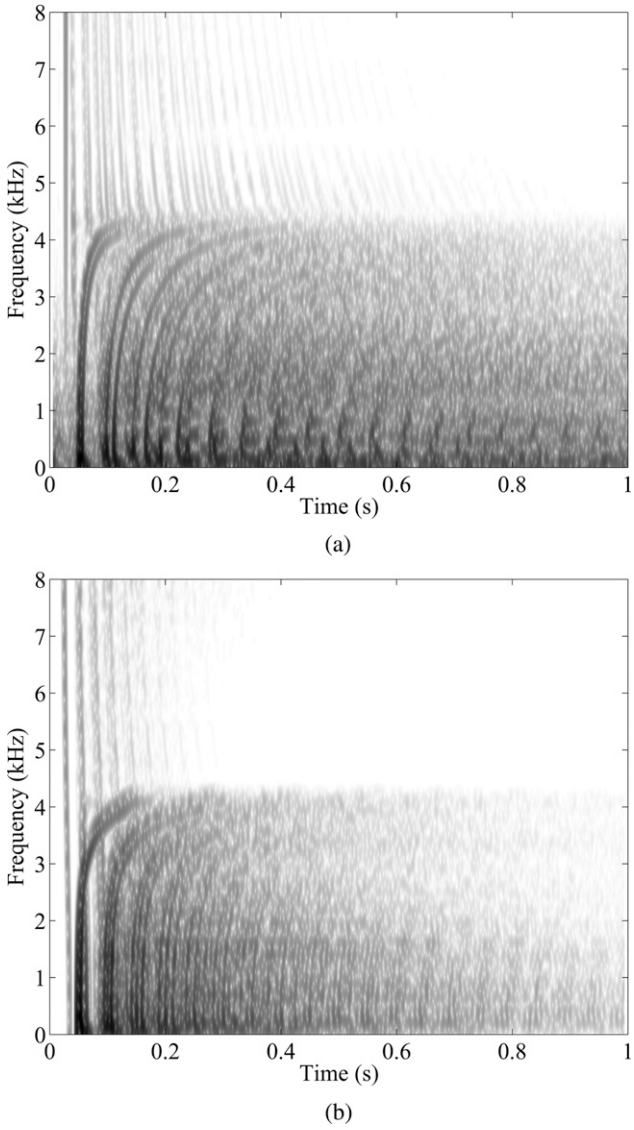

Fig. 24. Spectrograms of impulse responses. (a) Measured unit having three parallel springs. (b) Simulation of (a).

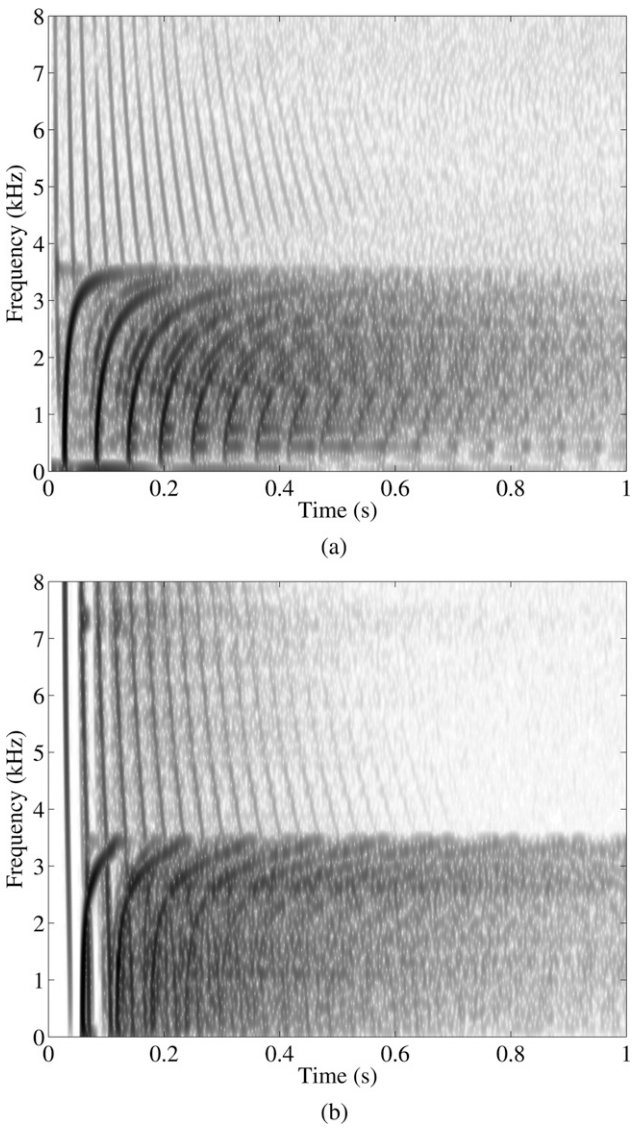

Fig. 25. Spectrograms of impulse responses. (a) Sansui RA-700 single-spring unit. (b) Simulation of (a).

of the low-frequency chirp sequence. With the exception of this problem, the agreement between the modeled and measured responses is good, both perceptually and via inspection of the spectrogram.

4 CONCLUSION

A parametric model for the simulation of spring reverberation units was introduced. A computationally efficient model that is easy to design was proposed for the chirps appearing in spring reverberation responses. The basic model consists of a spectral delay filter that is placed in a feedback loop together with a long delay line and a loop gain coefficient. Two separate sequences of chirps appear in the impulse response of a helical spring, one at low and another mostly at high frequencies. Two individual feedback structures are used for producing them.

For the low-frequency pulses a spectral delay filter based on interpolated stretched all-pass filters developed in this work is used. These new filters are obtained from a conventional first-order all-pass section by replacing the unit delay with an interpolated delay line, where the fractional delay is implemented with another first-order all-pass filter. This special all-pass filter produces several simultaneous image chirps, but only the lowest one in frequency is selected by removing the extra images with a low-pass filter.

A modulation technique was introduced in the feedback loop—the length of the delay line is modulated with a strongly correlated random-number sequence. This is implemented using time-varying linear interpolation. The delay modulation technique brings about a desirable blur to the dispersive pulses, which sounds similar to the reverberant tail heard in spring reverberation responses.

Faithful modeling of the series of chirps appearing at high frequencies is more tedious than that at low frequencies. However, it is sufficient to imitate the high-frequency chirp only above the transition frequency. In that case the high-frequency chirps can be synthesized with roughly the same amount of processing as lower frequencies. Perceptually the low-frequency pulses are more important than the high-frequency pulses because they are stronger and appear at the most sensitive range for the human hearing, below about 4 kHz.

Several parametric spring models can be connected in parallel to mimic practical spring units, which contain several springs. Model parameters, such as delay time, chirp shape, or decay rate, can be adjusted to obtain a rich variety of synthetic responses. This is an advantage in comparison to mechanical spring reverberation units, which cannot be modified as freely.

5 ACKNOWLEDGMENT

The authors would like to thank Universal Audio, Inc., for providing the Sansui RA-700 data set for this work. Part of this research was conducted in spring 2009 when Vesa Välimäki was a visiting scholar at CCRMA, Stanford University, Stanford, CA. This work has been supported by the Academy of Finland under projects 122815 and 126310.

6 REFERENCES

[1] L. Hammond, "Electrical Musical Instrument," US patent 2,230,836 (1941 Feb. 4).

[2] J. S. Abel, D. P. Berners, S. Costello, and J. O. Smith III, "Spring Reverb Emulation Using Dispersive Allpass Filters in a Waveguide Structure," presented at the 121st Convention of the Audio Engineering Society, *J. Audio Eng. Soc. (Abstracts)*, vol. 54, p. 1277 (2006 Dec.), convention paper 6954.

[3] J. S. Abel, K. Spratt, J. O. Smith, and D. P. Berners, "A Spring Reverb Model Employing Coupled Torsional and Longitudinal Modes," *IEEE Trans. Audio, Speech, Language Process.,* to be published (2010).

[4] J. Parker, "Spring Reverberation: A Finite Difference Approach," Master's thesis, University of Edinburgh, Edinburgh, UK (2008).

[5] S. Bilbao and J. Parker, "A Virtual Model of Spring Reverberation," *IEEE Trans. Audio, Speech, Language Process.*, vol. 18, pp. 799–808 (2010 May).

[6] M. R. Schroeder, "Natural Sounding Artificial Reverberation," *J. Audio Eng. Soc.*, vol. 10, pp. 219–223 (1962).

[7] J. A. Moorer, "About This Reverberation Business," *Computer Music J.*, vol. 3, pp. 13–28 (1979 June).

[8] J. M. Jot and A. Chaigne, "Digital Delay Networks for Designing Artificial Reverberators," presented at the 90th Convention of the Audio Engineering Society, *J. Audio Eng. Soc. (Abstracts)*, vol. 39, p. 383 (1991 May), preprint 3030.

[9] D. Griesinger, "Practical Processors and Programs for Digital Reverberation," in *Proc. AES 7th Int. Conf. on Audio in Digital Times* (Toronto, Ont., Canada, 1989 May), pp. 187–195.

[10] W. G. Gardner, "Reverberation Algorithms," in *Applications of Digital Signal Processing to Audio and Acoustics*, M. Kahrs and K. Brandenburg, Eds. (Kluwer Academic, Norwell, MA, 1997), pp. 85–131.

[11] S. Bilbao, "A Digital Plate Reverberation Algorithm," *J. Audio Eng. Soc.*, vol. 55, pp. 135–144 (2007 Mar).

[12] J. S. Abel, D. P. Berners, and A. Greenblatt, "An Emulation of the EMT140 Plate Reverberator Using a Hybrid Reverberator Structure," presented at the 127th Convention of the Audio Engineering Society, (Abstracts) www.aes.org/events/127/127thWrapUp.pdf, (2009 Oct.), convention paper 7928.

[13] S. Arnardottir, J. S. Abel, and J. O. Smith, "A Digital Model of the Echoplex Tape Delay," presented at the 125th Convention of the Audio Engineering Society, (Abstracts) www.aes.org/events/125/125thWrapUp.pdf, (2008 Oct.), convention paper 7649.

[14] A. Farina, "Simultaneous Measurement of Impulse Response and Distortion with a Swept-Sine Technique," presented at the 108th Convention of the Audio Engineering Society, *J. Audio Eng. Soc. (Abstracts)*, vol. 48, p. 350 (2000 Apr.), preprint 5093.

[15] J. Parker and S. Bilbao, "Spring Reverberation: A Physical Perspective," in *Proc. Int. Conf. on Digital Audio Effects (DAFx-09)* (Como, Italy, 2009 Sept.).

[16] V. Välimäki, J. S. Abel, and J. O. Smith, "Spectral Delay Filters," *J. Audio Eng. Soc.*, vol. 57, pp. 521–531 (2009 July/Aug.).

[17] J. O. Smith, *Spectral Audio Signal Processing* (W3K Publishing, 2009), http://www.w3k.org/books.

[18] T. I. Laakso, V. Välimäki, M. Karjalainen, and U. K. Laine, "Splitting the Unit Delay—Tools for Fractional Delay Filter Design," *IEEE Signal Process. Mag.*, vol. 13, pp. 30–60 (1996 Jan.).

[19] D. A. Jaffe and J. O. Smith, "Extensions of the Karplus–Strong Plucked-String Algorithm," *Computer Music J.*, vol. 7, no. 2, pp. 56–69 (1983).

[20] S. K. Mitra and K. Hirano, "Digital All-Pass Networks," *IEEE Trans. Circuits Sys.*, vol. 21, pp. 688–700 (1974 Sept.).

[21] J. O. Smith and J. B. Angell, "A Constant-Gain Digital Resonator Tuned by a Single Coefficient," *Computer Music J.*, vol. 6, no. 4, pp. 36–40 (1982).

[22] K. Steiglitz, "A Note on Constant-Gain Digital Resonators," *Computer Music J.*, vol. 18, no. 4, pp. 8–10 (1994).

[23] J. Pekonen, V. Välimäki, J. S. Abel, and J. O. Smith, "Spectral Delay Filters with Feedback and Time-Varying Coefficients," in *Proc. 12th Int. Conf. on Digital Audio Effects (DAFx-09)* (Como, Italy, 2009 Sept.).

[24] J. Pekonen and V. Välimäki, "Filter-Based Alias Reduction in Classical Waveform Synthesis," in *Proc. IEEE Int. Conf. on Acoustics, Speech and Signal Processing (ICASSP'08)* (Las Vegas, NV, 2008 Mar. 30–Apr. 4), pp. 133–136.

[25] V. Välimäki, H. Penttinen, J. Knif, M. Laurson, and C. Erkut, "Sound Synthesis of the Harpsichord Using a Computational Efficient Physical Model," *EURASIP J. Appl. Signal Process.*, vol. 2004, pp. 934–948 (2004).

[26] J. Dattorro, "Effect Design—Part II: Delay-Line Modulation and Chorus," *J. Audio Eng. Soc.*, vol. 45, pp. 764–788 (1997 Oct.).

[27] J. Dattorro, "Effect Design—Part 1: Reverberator and Other Filters," *J. Audio Eng. Soc.*, vol. 45, pp. 660–684 (1997 Sept.).

[28] J. Frenette, "Reducing Artificial Reverberation Requirements Using Time-Variant Feedback Delay Networks," Master's thesis, University of Miami, Coral Gables, FL (2000 Dec.).

[29] J. G. Proakis and D. G. Manolakis, *Digital Signal Processing—Principles, Algorithms and Application*, 4th ed. (Pearson Prentice–Hall, Upper Saddle River, NJ, 2007), pp. 595–596.

[30] T. I. Laakso and V. Välimäki, "Energy-Based Effective Length of the Impulse Response of a Recursive Filter," *IEEE Trans. Instrum. Meas.*, vol. 48, pp. 7–17 (1999 Feb.).

THE AUTHORS

V. Välimäki

J. D. Parker

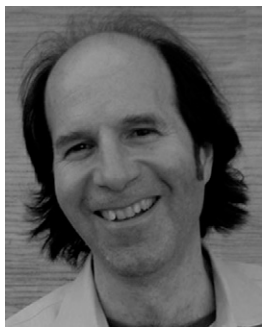

J. S. Abel

Vesa Välimäki received a Master of Science degree in technology, Licentiate of Science in technology, and Doctor of Science in technology in electrical engineering from the Helsinki University of Technology (TKK), Espoo, Finland, in 1992, 1994, and 1995, respectively. His doctoral dissertation dealt with fractional delay filters and physical modeling of musical wind instruments.

Since 1990 he has been working mostly at TKK, with the exception of a few periods. He is presently professor of audio signal processing at the Aalto University. In 1996 he spent six months as a postdoctoral research fellow at the University of Westminster, London, UK. In 2001–2002 he was professor of signal processing at the Pori School of Technology and Economics, Tampere University of Technology, Pori, Finland. During the academic year 2008–2009 he was on sabbatical leave and spent several months as a visiting scholar at the Center for Computer Research in Music and Acoustics (CCRMA), Stanford University, Stanford, CA. His research interests include musical signal processing, digital filter design, and acoustics of musical instruments.

Dr. Välimäki is a senior member of the IEEE Signal Processing Society and a member of the Audio Engineering Society, the Acoustical Society of Finland, and the Finnish Musicological Society. He was the chairman of the 11th International Conference on Digital Audio Effects (DAFx-08), which was held in Espoo, Finland, in 2008.

●

Julian D. Parker was born in the UK in 1982. He started his academic life as a physicist, receiving a B.A. degree in natural sciences from Clare College, Cambridge, UK, in 2005, and then an M.Sc. degree in acoustics and music technology from the University of Edinburgh, UK. He is

currently studying for his doctoral degree at Aalto University in Espoo, Finland. His research interests focus on unconventional methods of musical audio processing and synthesis utilizing systems exhibiting highly dispersive or nonlinear behavior.

●

Jonathan S. Abel received M.S. and Ph.D. degrees from Stanford University, Stanford, CA, and an S.B. degree from the Massachusetts Institute of Technology, Cambridge, MA, all in electrical engineering.

From 1999 to 2007 he was a cofounder and chief technology officer of the Grammy Award–winning Universal Audio, Inc. He was a researcher at NASA/Ames Research Center, exploring topics in room acoustics and spatial hearing on a grant through the San Jose State University Foundation. He was also chief scientist at Crystal River Engineering, Inc., where he developed their positional audio technology, and a lecturer in the Department of Electrical Engineering at Yale University. At present he is a consulting professor at the Center for Computer Research in Music and Acoustics (CCRMA) in the Music Department at Stanford University where his research interests include audio and music applications of signal and array processing, parameter estimation, and acoustics. As an industry consultant, he was worked with Apple, FDNY, LSI Logic, NRL, SAIC and Sennheiser on projects in professional audio, GPS, medical imaging, passive sonar and fire department resource allocation.

Dr. Abel is a Fellow of the Audio Engineering Society.